An Interacting Multiple Model Estimator of LEO Satellite Clocks for Improved Positioning

Nadim Khairallah and Zaher M. Kassas
Department of Mechanical and Aerospace Engineering, University of California, Irvine, USA
Emails: khairaln@uci.edu and zkassas@ieee.org

***Abstract*—An interacting multiple-model (IMM) estimator is developed to adaptively estimate the process noise covariance of low Earth orbit (LEO) satellite clocks for improved positioning. Experimental results are presented showing a stationary ground receiver localizing itself with carrier phase measurements from a single Orbcomm LEO satellite. The developed IMM is shown to reduce the localization error and improve filter consistency over two fixed mismatched extended Kalman filters (EKFs). Starting with an initial receiver position error of 1.45 km, the IMM yielded a final error of 111.26 m, while the errors of a conservative and optimistic EKFs converged to 254.71 m and 429.35 m, respectively.**

***Index Terms*—IMM, navigation, signals of opportunity, low Earth orbit satellites, adaptive estimation.**

I. Introduction

Opportunistic navigation has gained significant attention in recent years to overcome the limitations of global navigation satellite systems (GNSS). This paradigm aims to exploit ambient signals of opportunity (SOPs) in the environment [1], [2]. Various generations of terrestrial cellular signals (3G code-division multiple-access (CDMA), 4G long-term evolution (LTE), and 5G [3]–[6]), have shown the potential of meter-level level accuracy on ground and aerial vehicles [7]–[9]. As for space-based SOPs, low Earth orbit (LEO) space vehicles (SVs) have received significant attention recently, as they could revolutionize satellite-based navigation [10]–[17].

LEO SVs' inherent characteristics make them desirable for navigation. First, LEO SVs are abundant, with around 3,800 active SVs in orbit. The number of LEO SVs is projected to increase dramatically over this decade due to the launch of so-called megaconstellations (e.g., Starlink, Kuiper, etc.) [18]. Second, LEO SVs' configuration relative to a receiver anywhere on Earth yields a low geometric dilution of precision (GDOP), which improves navigation accuracy [19]. Third, LEO SVs transmit in a wide range of frequency bands (e.g., Orbcomm SVs transmit in the very-high frequency band, while Starlink SVs transmit in the Ku-band), which reduces vulnerability to interference. Fourth, LEO SVs are around twenty times closer to Earth than GNSS SVs, which reside in medium Earth orbit (MEO), making the power of received LEO signals up to 2,400 times more powerful than GNSS [20].

However, there are two main challenges to opportunistic navigation using LEO SVs. First, the proprietary signals transmitted by LEO SVs are partially known. This issue can be tackled with the design of specialized receivers that leverage the periodic signals with favorable correlation properties transmitted by the LEO SVs [21], [22]. Even when LEO signals are unknown, cognitive signal processing approaches have been shown to yield useful navigation observables [23], [24]. Second, unlike GNSS SVs, LEO SVs generally do not openly transmit information about their ephemeris and clock error states in their downlink signals. On one hand, among the most accurate publicly available information on ephemerides are two-line element (TLE) file, published and updated periodically by the North American Aerospace Defense Command (NORAD) [25]. These TLE files consist of a set of mean Keplerian elements at a specified epoch that an analytical Simplified General Perturbation (SGP4) model [26] can propagate to any inquiry time. TLEs, however, suffer from errors of a few kilometers at epoch and this error grows throughout propagation. On the other hand, the quality of oscillators onboard LEO SVs is generally unknown and no information is available on the degree of synchronicity of clocks across the constellation network.

As such, LEO SVs' states are uncertain at best (ephemeris) or completely unknown (clock errors). One approach to deal with this is via the simultaneous tracking and navigation (STAN) framework, which estimates the SVs' states simultaneously with the receiver's states [11], [27]. Another approach was proposed in [28], in which LEO SVs' position and velocity process noise was estimated by a receiver, which tracked the LEO SVs by utilizing pseudorange and/or Doppler measurements from LEO SVs' signals.

This paper focuses on the challenge of estimating the process noise covariance of unknown LEO SVs' clocks. Prior work in the context of mapping unknown cellular towers with a mobile ground-based receiver has demonstrated that adaptive estimation of terrestrial SOP clocks improves the estimation performance [29]. This paper considers a "dual" problem in which a stationary receiver localizes itself from signals transmitted by a single LEO SV, while adaptively estimating the unknown clock of the SV. To this end, an interacting multiple-model (IMM) estimator, which uses a bank of extended Kalman filters (EKFs), is developed. IMMs have shown tremendous potential in a variety of applications [30], [31] and have been "adapted" to estimating process and measurement noise statistics [32].

The rest of the paper is organized as follows. Section II presents the clock dynamics and measurement models. Section III details the estimation framework to adaptively localize a stationary receiver using LEO SVs. Section IV presents

experimental results. Section V gives concluding remarks.

II. Model Description

A. Clock Dynamics Model

The receiver and LEO SV clock error states are modeled according to the standard double integrator model with bias δt and drift $\dot{\delta t}$, which evolve according to

$$\dot{\boldsymbol{x}}_{\text{clk}}(t) = \mathbf{A}_{\text{clk}}\, \boldsymbol{x}_{\text{clk}}(t) + \tilde{\boldsymbol{w}}_{\text{clk}}(t), \tag{1}$$

$$\boldsymbol{x}_{\text{clk}} = \begin{bmatrix} \delta t \\ \dot{\delta t} \end{bmatrix}, \quad \tilde{\boldsymbol{w}}_{\text{clk}} = \begin{bmatrix} \tilde{w}_{\delta t} \\ \tilde{w}_{\dot{\delta t}} \end{bmatrix}, \quad \mathbf{A}_{\text{clk}} = \begin{bmatrix} 0 & 1 \\ 0 & 0 \end{bmatrix},$$

where $\tilde{w}_{\delta t}$ and $\tilde{w}_{\dot{\delta t}}$ are zero-mean, mutually independent white noise processes with power spectral density $S_{\tilde{w}_{\delta t}}$ and $S_{\tilde{w}_{\dot{\delta t}}}$, respectively. These power spectra $S_{\tilde{w}_{\delta t}}$ and $S_{\tilde{w}_{\dot{\delta t}}}$ can be related to the power-law coefficients $\{h_\alpha\}_{\alpha=-2}^{2}$, which have been shown through laboratory experiments to be adequate to characterize the power spectral density of the fractional frequency deviation $y(t)$ of an oscillator from nominal frequency, which takes the form $S_y(f) = \sum_{\alpha=-2}^{2} h_\alpha f^\alpha$ [33]. It is common to approximate the clock error dynamics by considering only the frequency random walk coefficient h_{-2} and the white frequency coefficient h_0, which lead to $S_{\tilde{w}_{\delta t}} \approx \frac{h_0}{2}$ and $S_{\tilde{w}_{\dot{\delta t}}} \approx 2\pi^2 h_{-2}$ [34].

Discretizing (1) at a constant sampling period T yields

$$\boldsymbol{x}_{\text{clk}}(k+1) = \mathbf{F}_{\text{clk}}\, \boldsymbol{x}_{\text{clk}}(k) + \boldsymbol{w}_{\text{clk}}(k), \quad k = 0, 1, 2, \ldots \tag{2}$$

where $\boldsymbol{w}_{\text{clk}}$ is a zero-mean white noise sequence with covariance $\mathbf{Q}_{\text{clk}}$

$$\mathbf{Q}_{\text{clk}} = \begin{bmatrix} S_{\tilde{w}_{\delta t}} T + S_{\tilde{w}_{\dot{\delta t}}} \frac{T^3}{3} & S_{\tilde{w}_{\dot{\delta t}}} \frac{T^2}{2} \\ S_{\tilde{w}_{\dot{\delta t}}} \frac{T^2}{2} & S_{\tilde{w}_{\dot{\delta t}}} T \end{bmatrix}, \; \mathbf{F}_{\text{clk}} = \begin{bmatrix} 1 & T \\ 0 & 1 \end{bmatrix}. \tag{3}$$

B. Carrier Phase Measurement Model

The receiver opportunistically extracts carrier phase navigation observables from the LEO SV signals. These carrier phase measurements between the receiver and the m^{th} LEO SV at time-step k corresponding to time $t_k = t_0 + kT$ for some initial time t_0 are modeled according to

$$\begin{aligned} z_m(k) = {} & \|\boldsymbol{r}_r(k) - \boldsymbol{r}_{\text{sv}_m}(k')\|_2 + c\left[\delta t_r(k) - \delta t_{\text{sv}_m}(k')\right] \\ & + \lambda_m N_m + c\delta t_{\text{tropo}_m}(k) + c\delta t_{\text{iono}_m}(k) + v_m(k), \end{aligned} \tag{4}$$

where k' is the time-step corresponding to $t_{k'} = t_k - \delta_{\text{TOF}}$ with δ_{TOF} being the true time-of-flight of the signal from the m^{th} LEO SV to the receiver; $\boldsymbol{r}_r \triangleq [x_r, y_r, z_r]^\mathsf{T}$ and $\boldsymbol{r}_{\text{sv}_m} \triangleq [x_{\text{sv}_m}, y_{\text{sv}_m}, z_{\text{sv}_m}]^\mathsf{T}$ are the receiver's and m^{th} LEO SV's 3-D position, respectively, expressed in the Earth-centered, Earth-fixed (ECEF) reference frame; c is the speed of light; δt_r and δt_{sv_m} are the receiver's and the m^{th} LEO SV's clock bias, respectively; λ_m is the m^{th} LEO SV's carrier wavelength; N_m is the m^{th} LEO SV's carrier phase ambiguity; $\delta t_{\text{tropo}_m}$ and δt_{iono_m} are the tropospheric and ionospheric delays associated with the m^{th} LEO SV's signals, respectively; and $v_m(k)$ is the measurement noise, which is modeled as a zero-mean white Gaussian sequence with variance $\sigma_m^2(k)$.

Assuming no cycle slip occurs when the receiver tracks the carrier phase (i.e., the carrier phase ambiguity remains constant), the difference between the receiver and the m^{th} LEO SV range-equivalent clock biases and the range-equivalent carrier phase ambiguity are lumped into a single term $c\Delta\delta t_m(k)$, simplifying the carrier phase measurement model to

$$\begin{aligned} z_m(k) = {} & \|\boldsymbol{r}_r(k) - \boldsymbol{r}_{\text{sv}_m}(k')\|_2 + c\Delta\delta t_m(k) \\ & + c\delta t_{\text{tropo}_m}(k) + c\delta t_{\text{iono}_m}(k) + v_m(k), \end{aligned} \tag{5}$$

$$c\Delta\delta t_m(k) \triangleq c\left[\delta t_r(k) - \delta t_{\text{sv}_m}(k')\right] + \lambda_m N_m. \tag{6}$$

III. Adaptive Estimation Framework

In multiple-model (MM) estimation, a bank of filters, traditionally Kalman filters (KFs), run in parallel, with each filter in the bank matched to a mode. The output of the MM estimator is obtained by weighing each filter's estimate by their respective innovation likelihood [34]. For systems modeled with Markovian switching probabilities between modes, the computational cost of the exhaustive MM estimator, which keeps track of all mode combinations, grows exponentially with time. Several sub-optimal filters such as the generalized pseudo-Bayesian (GPB) algorithms have been developed to remedy this issue by considering the one-step time history for GPB1 (r hypotheses) and two-step time history for GPB2 (r^2 hypotheses), where r is the number of modes [34]. The interacting multiple-model (IMM) was developed to allow for a two-step history processing using only r filters running in parallel via a mixing stage that computes the initial condition fed to each filter. As a result, the IMM, which has the computational cost of GPB1 but with comparable performance to GPB2, offers a tradeoff between complexity and adaptation capability [35], and is selected as the adaptive filter used in this study.

A single cycle of the IMM for r modes is depicted in Fig. 1, with the following notational definitions:

r	Number of filters
i	$\{1, \ldots, r\} \in \mathbb{N}$
$\hat{\boldsymbol{x}}^i(k-1\|k-1)$	State estimate of filter i
$\mathbf{P}^i(k-1\|k-1)$	Estimation error covariance of filter i
$\mathbf{M}(k-1\|k-1)$	Mixing probability matrix
$\hat{\boldsymbol{x}}^{0i}(k-1\|k-1)$	Mixed initial condition matched to filter i
$\mathbf{P}^{0i}(k-1\|k-1)$	Estimation error covariance associated with $\hat{\boldsymbol{x}}^{0i}(k-1\|k-1)$
$\boldsymbol{z}(k)$	Measurement
$\Lambda_i(k)$	Innovation likelihood of filter i
$\hat{\boldsymbol{x}}^i(k\|k)$	Updated state estimate of filter i
$\mathbf{P}^i(k\|k)$	Updated estimation error covariance of filter i
$\boldsymbol{\pi}$	Mode transition probability matrix
$\boldsymbol{\mu}(k)$	Mode probability vector
$\hat{\boldsymbol{x}}(k\|k)$	Combined state estimate
$\mathbf{P}(k\|k)$	Combined estimation error covariance

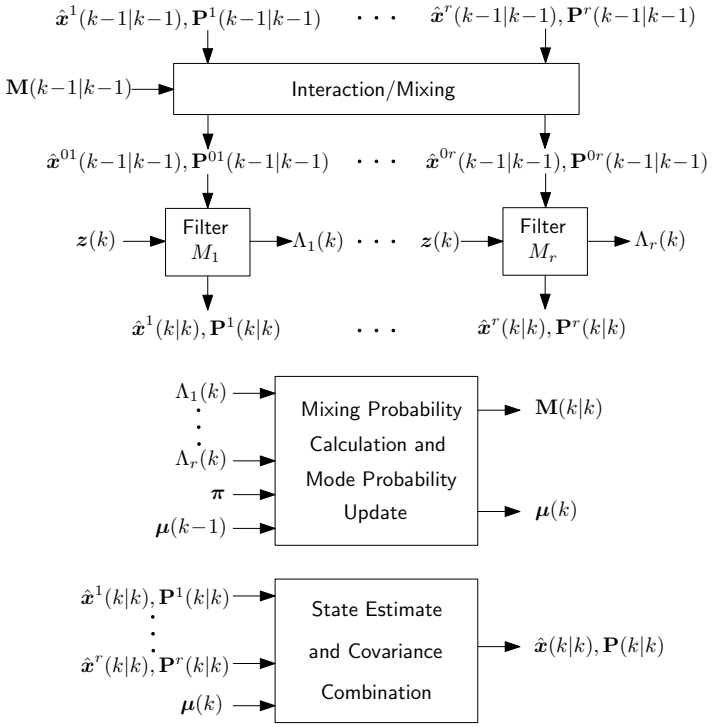

Fig. 1. A single cycle of the IMM filter with r modes.

The IMM algorithm consists of the four following stages, shown in Fig. 1, repeated recursively:

Interaction/mixing: This stage calculates the initial conditions $\hat{\boldsymbol{x}}^{0i}(k{-}1|k{-}1)$ and $\mathbf{P}^{0i}(k{-}1|k{-}1)$ fed to each filter in the bank by combining $\hat{\boldsymbol{x}}^{i}(k{-}1|k{-}1)$ and $\mathbf{P}^{i}(k{-}1|k{-}1)$ using the mixing probability matrix $\mathbf{M}(k{-}1|k{-}1)$.

Mode-matched filtering: This stages performs a regular KF update (prediction and correction), for each KF in the bank, where each filter is matched to a particular mode. It also calculates the innovation likelihood of each filter.

Mixing probability and mode probability update: This stage computes the mixing probability matrix and updates the mode probability vector, based on the innovation likelihood of each filter in the bank.

State estimate and covariance combination: This stage combines the state estimates and estimation error covariances from the individual filters by weighting $\hat{\boldsymbol{x}}^{i}(k|k)$ and $\mathbf{P}^{i}(k|k)$ by their respective mode probabilities from $\boldsymbol{\mu}(k)$.

In this study, an IMM adaptive filter is implemented to estimate the clock error states' process noise covariance online to improve the positioning of an unknown receiver.

The process noise covariance of the clock error states depends on the corresponding oscillator stability. The quality of oscillators vary widely between temperature-compensated crystal oscillator (TCXO), oven-controlled crystal oscillator (OCXO), and chip-scale atomic clock (CSAC). The discrete-time process noise covariance for clock error states is readily calculated from (3), where the power spectral densities $S_{\tilde{w}_{\delta t}}$ and $S_{\tilde{w}_{\delta_t}}$ depend on the power-law coefficients associated with the oscillator stability. Table I summarizes the power-law coefficients of various clock qualities.

The process noise covariance $\mathbf{Q}$ associated with the range-equivalent lumped term (6) only depends on the receiver's and LEO SV's stochastic clock error states as the range-equivalent carrier phase ambiguity is deterministic, and is given by

$$\mathbf{Q} = c^2 \left[\mathbf{Q}_{\mathrm{clk}_r} + \mathbf{Q}_{\mathrm{clk}_{\mathrm{sv}}}\right], \tag{7}$$

where $\mathbf{Q}_{\mathrm{clk}_r}$ and $\mathbf{Q}_{\mathrm{clk}_{\mathrm{sv}}}$ are computed from (3) by using the receiver's and LEO SV's oscillator power spectra, respectively.

TABLE I
CLOCK QUALITY POWER-LAW COEFFICIENT VALUES.

Quality	Coefficients $\{\boldsymbol{h_0}, \boldsymbol{h_{-2}}\}$
Worst TCXO	$\{2.0 \times 10^{-19}, 2.0 \times 10^{-20}\}$
Typical TCXO	$\{9.4 \times 10^{-20}, 3.8 \times 10^{-21}\}$
Typical OCXO	$\{8.0 \times 10^{-20}, 4.0 \times 10^{-23}\}$
Best OCXO	$\{2.6 \times 10^{-22}, 4.0 \times 10^{-26}\}$
CSAC	$\{7.2 \times 10^{-21}, 2.7 \times 10^{-27}\}$

IV. Experimental Results

To demonstrate the improvements in receiver positioning accuracy and filter consistency, achieved via the adaptation in the IMM over mismatched EKFs, Orbcomm SV signals were collected by a stationary receiver. Orbcomm was chosen for this experiment since its SVs openly transmit ephemeris information in their downlink signals [36]. The ephemeris data was decoded by the receiver and used in the estimators as the SV's ground truth trajectory.

A. Experimental Setup and Filter Parameters

A VHF quadrifilar helix antenna was connected to an Ettus E312 Universal Software Radio Peripheral (USRP) disciplined by a NI CDA-2990 OctoClock to sample Orbcomm LEO SV signals at 137-138 MHz at a sampling rate of 2.4 MSps.

An IMM estimator and two fixed mismatched EKFs were implemented to estimate the receiver's position and the lumped term (6) and its rate of change. It is assumed that the receiver has knowledge of its height (e.g., through altimeter measurements) so that the filters effectively estimate the receiver's planar two-dimensional position in a local North-East-Down (NED) frame.

It is hypothesized that the receiver's clock quality lies between a worst TCXO and a best OCXO and that the LEO SV's clock quality lies between a typical TCXO and a CSAC. As a result, the IMM filter runs $r = 4$ different modes, one for each possible combination of receiver-LEO SV clock quality. The IMM filter is initialized with $\mu_i(0) = 1/r,\ i = 1, \ldots, r$ as no prior is available on the oscillators' stability and the Markovian mode transition matrix is given by $\boldsymbol{\pi}_{ij} = \begin{cases} 1-p, & \text{if } i = j = 1, \ldots, r \\ p/(r-1), & \text{if } i \neq j \end{cases}$ where p is the probability of transition to another mode, which is set to 10^{-4}.

The IMM's performance is also compared to that of two mismatched EKFs: a conservative filter which overbounds $\mathbf{Q}$ by assuming a receiver-LEO SV joint clock quality equivalent to a worst TCXO-typical TCXO pair and an optimistic filter which underestimates $\mathbf{Q}$ by assuming a receiver-LEO SV joint clock quality equivalent to a typical OCXO-best OCXO pair.

B. Experimental Results

The USRP sampled downlink signals from Orbcomm FM116 SV for around 4.5 minutes. Carrier phase navigation observables were opportunistically extracted by the receiver and were corrected for tropospheric and ionospheric delays using standard models [37]. The measurement noise variance was time-varying and was calculated based on the LEO SV's elevation angle. All filters were initialized with the same initial receiver position estimate, drawn from a Gaussian distribution with the mean being the true receiver's location and a variance of 10^6 m^2 in the North and East directions as seen in Fig. 2. The initial receiver position error was 1.45 km.

Fig. 2 and Table II summarize the receiver localization performance of the IMM and the two fixed EKFs. The following observations can be drawn from these results. First, the IMM yielded better localization performance than the two mismatched EKFs by decreasing the initial positioning error from 1.45 km to 111.26 m versus 254.71 m and 429.35 m for the conservative and optimistic EKFs, respectively. Second, the IMM's covariance captures well the uncertainty in the positioning error whereas the uncertainty for the EKF overbounding $\mathbf{Q}$ is too conservative and the uncertainty for the EKF underestimating $\mathbf{Q}$ is too optimistic. The above observations can be explained by the fact that mismatched process noise covariances lead to less accurate estimates and filter inconsistency or even divergence as in the case of the optimistic EKF [29]. The adaptation capability of the IMM filter addresses the unknown process noise covariance by estimating it online along the receiver position states. Third, the uncertainty ellipses of all three filters are elongated in the same direction as can be seen in Fig. 2(a). This is explained by the motion of the LEO SV relative to the receiver: more information is available in the direction parallel to the LEO SV's motion, resulting in more uncertainty (i.e., elongated covariance ellipses) in the direction orthogonal to the LEO SV's trajectory depicted in the skyplot of Fig. 2(b).

Fig. 3 shows the time evolution of the IMM mode probabilities and suggests that the combined receiver-LEO SV clocks have comparable stability to a typical TCXO-best OCXO oscillator pair.

If a cycle slip occurs in the carrier phase observables, a sharp step equal to the number of cycles slipped multiplied by the carrier wavelength is suddenly introduced in the time evolution of the lumped term (6). This step will act as a disturbance to any filter estimating (6). It is expected that after the transient period following the cycle slip disturbance, the IMM mode probabilities converge back to the values that correctly characterize the clock error states' process noise covariance.

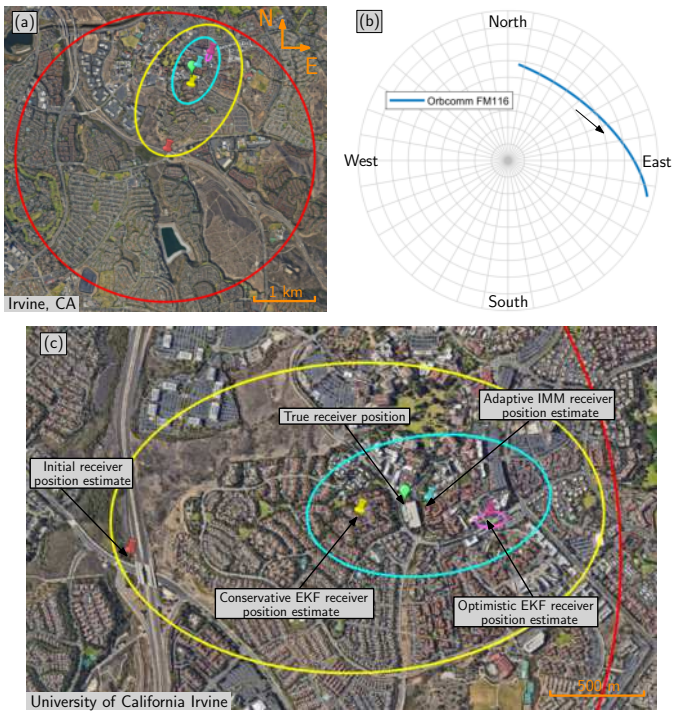

Fig. 2. (a) Experimental results showing true receiver position (green) along with estimates and corresponding 95^{th}-percentile uncertainty ellipses: (i) red: initial estimate, (ii) yellow: conservative EKF, (iii) purple: optimistic EKF, and (iv) blue: IMM. (b) Skyplot of Orbcomm FM116 SV's trajectory relative to the receiver. (c) Zoomed view on the localization performance of different filters. Map data: Google Earth.

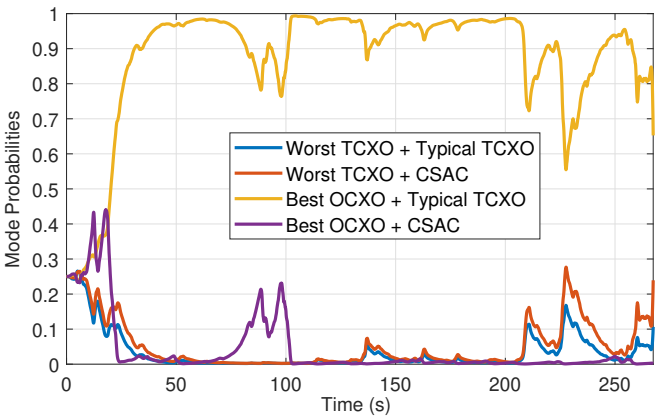

Fig. 3. IMM mode probabilites.

TABLE II
COMPARISON OF IMM VERSUS MISMATCHED FIXED EKFS.

	Adaptive IMM	Conservative EKF	Optimistic EKF
Final error (m)	111.26	254.71	429.35

V. CONCLUSION

This paper developed an IMM estimator to localize a receiver using carrier phase measurements extracted from a single LEO SV's signals. The IMM adaptively estimated the process noise covariance of the combined receiver-LEO SV clock error states. The accuracy and consistency advantages of

the IMM adaptation were showcased experimentally against two fixed mismatched EKFs. The IMM reduced the initial receiver position error from 1.45 km to 111.26 m, while a conservative EKF yielded a final error of 254.71 m and an optimistic EKF diverged to an error of 429.35 m.

ACKNOWLEDGMENTS

This work was supported in part by the Office of Naval Research (ONR) under Grant N00014-19-1-2511 and Grant N00014-19-1-2613, in part by the National Science Foundation (NSF) under Grant 1929965, and in part by the U.S. Department of Transportation (USDOT) under Grant 69A3552047138 for the CARMEN University Transportation Center (UTC). The authors would like to thank Sharbel Kozhaya for his help with data collection and processing.

REFERENCES

[1] J. Raquet *et al.*, "Position, navigation, and timing technologies in the 21st century," J. Morton, F. van Diggelen, J. Spilker, Jr., and B. Parkinson, Eds. Wiley-IEEE, 2021, vol. 2, Part D: Position, Navigation, and Timing Using Radio Signals-of-Opportunity, ch. 35–43, pp. 1115–1412.

[2] N. Souli, P. Kolios, and G. Ellinas, "Online relative positioning of autonomous vehicles using signals of opportunity," *IEEE Transactions on Intelligent Vehicles*, pp. 1–1, 2021.

[3] J. Khalife and Z. Kassas, "Navigation with cellular CDMA signals – part II: Performance analysis and experimental results," *IEEE Transactions on Signal Processing*, vol. 66, no. 8, pp. 2204–2218, April 2018.

[4] P. Wang and Y. Morton, "Multipath estimating delay lock loop for LTE signal TOA estimation in indoor and urban environments," *IEEE Transactions on Wireless Communications*, vol. 19, no. 8, pp. 5518–5530, 2020.

[5] J. Gante, L. Sousa, and G. Falcao, "Dethroning GPS: Low-power accurate 5G positioning systems using machine learning," *IEEE Journal on Emerging and Selected Topics in Circuits and Systems*, vol. 10, no. 2, pp. 240–252, June 2020.

[6] H. Dun, C. Tiberius, and G. Janssen, "Positioning in a multipath channel using OFDM signals with carrier phase tracking," *IEEE Access*, vol. 8, pp. 13 011–13 028, 2020.

[7] C. Yang, T. Nguyen, and E. Blasch, "Mobile positioning via fusion of mixed signals of opportunity," *IEEE Aerospace and Electronic Systems Magazine*, vol. 29, no. 4, pp. 34–46, April 2014.

[8] J. del Peral-Rosado, O. Renaudin, C. Gentner, R. Raulefs, E. Dominguez-Tijero, A. Fernandez-Cabezas, F. Blazquez-Luengo, G. Cueto-Felgueroso, A. Chassaigne, D. Bartlett, F. Grec, L. Ries, R. Prieto-Cerdeira, J. Lopez-Salcedo, and G. Seco-Granados, "Physical-layer abstraction for hybrid GNSS and 5G positioning evaluations," in *Proceedings of IEEE Vehicular Technology Conference*, September 2019, pp. 1–6.

[9] A. Abdallah and Z. Kassas, "UAV navigation with 5G carrier phase measurements," in *Proceedings of ION GNSS Conference*, September 2021, pp. 3294–3306.

[10] R. Landry, A. Nguyen, H. Rasaee, A. Amrhar, X. Fang, and H. Benzerrouk, "Iridium Next LEO satellites as an alternative PNT in GNSS denied environments–part 1," *Inside GNSS Magazine*, vol. 14, no. 3, pp. 56–64., May 2019.

[11] Z. Kassas, J. Morales, and J. Khalife, "New-age satellite-based navigation – STAN: simultaneous tracking and navigation with LEO satellite signals," *Inside GNSS Magazine*, vol. 14, no. 4, pp. 56–65, 2019.

[12] T. Reid, B. Chan, A. Goel, K. Gunning, B. Manning, J. Martin, A. Neish, A. Perkins, and P. Tarantino, "Satellite navigation for the age of autonomy," in *Proceedings of IEEE/ION Position, Location and Navigation Symposium*, 2020, pp. 342–352.

[13] Q. Wei, X. Chen, and Y. Zhan, "Exploring implicit pilots for precise estimation of LEO satellite downlink Doppler frequency," *IEEE Communications Letters*, vol. 24, no. 10, pp. 2270–2274, 2020.

[14] S. Thompson, S. Martin, and D. Bevly, "Single differenced Doppler positioning with low Earth orbit signals of opportunity and angle of arrival estimation," in *Proceedings of ION International Technical Meeting*, 2020, pp. 497–509.

[15] A. Nardin, F. Dovis, and J. Fraire, "Empowering the tracking performance of LEO'-based positioning by means of meta-signals," *IEEE Journal of Radio Frequency Identification*, pp. 1–1, 2021.

[16] R. Cassel, D. Scherer, D. Wilburne, J. Hirschauer, and J. Burke, "Impact of improved oscillator stability on LEO-based satellite navigation," in *Proceedings of ION International Technical Meeting*, January 2022, pp. 893–905.

[17] J. Khalife, M. Neinavaie, and Z. Kassas, "The first carrier phase tracking and positioning results with Starlink LEO satellite signals," *IEEE Transactions on Aerospace and Electronic Systems*, vol. 56, no. 2, pp. 1487–1491, April 2022.

[18] S. Liu, Z. Gao, Y. Wu, D. Kwan Ng, X. Gao, K. Wong, S. Chatzinotas, and B. Ottersten, "LEO satellite constellations for 5G and beyond: How will they reshape vertical domains?" *IEEE Communications Magazine*, vol. 59, no. 7, pp. 30–36, July 2021.

[19] Z. Kassas, M. Neinavaie, J. Khalife, N. Khairallah, J. Haidar-Ahmad, S. Kozhaya, and Z. Shadram, "Enter LEO on the GNSS stage: Navigation with Starlink satellites," *Inside GNSS Magazine*, vol. 16, no. 6, pp. 42–51, 2021.

[20] D. Lawrence, H. Cobb, G. Gutt, M. OConnor, T. Reid, T. Walter, and D. Whelan, "Navigation from LEO: Current capability and future promise," *GPS World Magazine*, vol. 28, no. 7, pp. 42–48, July 2017.

[21] F. Farhangian and R. Landry, "Multi-constellation software-defined receiver for Doppler positioning with LEO satellites," *Sensors*, vol. 20, no. 20, pp. 5866–5883, October 2020.

[22] C. Pinell, "Receiver architectures for positioning with low Earth orbit satellite signals," Master's thesis, Lulea University of Technology, School of Electrical Engineering, Sweden, 2021.

[23] M. Neinavaie, J. Khalife, and Z. Kassas, "Blind Doppler tracking and beacon detection for opportunistic navigation with LEO satellite signals," in *Proceedings of IEEE Aerospace Conference*, March 2021, pp. 1–8.

[24] M. Neinavaie, J. Khalife, and Z. Kassas, "Acquisition, Doppler tracking, and positioning with Starlink LEO satellites: First results," *IEEE Transactions on Aerospace and Electronic Systems*, 2021, accepted.

[25] North American Aerospace Defense Command (NORAD), "Two-line element sets," http://celestrak.com/NORAD/elements/.

[26] D. Vallado and P. Crawford, "SGP4 orbit determination," in *Proceedings of AIAA/AAS Astrodynamics Specialist Conference and Exhibit*, August 2008, pp. 6770–6799.

[27] S. Kozhaya, J. Haidar-Ahmad, A. Abdallah, Z. Kassas, and S. Saab, "Comparison of neural network architectures for simultaneous tracking and navigation with LEO satellites," in *Proceedings of ION GNSS Conference*, September 2021, pp. 2507–2520.

[28] N. Khairallah and Z. Kassas, "Ephemeris closed-loop tracking of LEO satellites with pseudorange and Doppler measurements," in *Proceedings of ION GNSS Conference*, September 2021, pp. 2544–2555.

[29] Z. Kassas, V. Ghadiok, and T. Humphreys, "Adaptive estimation of signals of opportunity," in *Proceedings of ION GNSS Conference*, September 2014, pp. 1679–1689.

[30] S. Kim, J. Choi, and Y. Kim, "Fault detection and diagnosis of aircraft actuators using fuzzy-tuning IMM filter," *IEEE Transactions on Aerospace and Electronic Systems*, vol. 44, no. 3, pp. 940–952, July 2008.

[31] M. Gomaa, O. De Silva, G. Mann, and G. Gosine, "Observability-constrained VINS for MAVs using interacting multiple model algorithm," *IEEE Transactions on Aerospace and Electronic Systems*, vol. 57, no. 3, pp. 1423–1442, June 2021.

[32] R. Li, X., and Y. Bar-Shalom, "A recursive multiple model approach to noise identification," *IEEE Transactions on Aerospace and Electronic Systems*, vol. 30, no. 3, pp. 671–684, July 1994.

[33] A. Thompson, J. Moran, and G. Swenson, *Interferometry and Synthesis in Radio Astronomy*, 2nd ed. John Wiley & Sons, 2001.

[34] Y. Bar-Shalom, X. Li, and T. Kirubarajan, *Estimation with Applications to Tracking and Navigation*. New York, NY: John Wiley & Sons, 2002.

[35] H. Blom and Y. Bar-Shalom, "The interacting multiple model algorithm for systems with Markovian switching coefficients," *IEEE Transactions on Automatic Control*, vol. 33, no. 8, pp. 780–783, August 1988.

[36] M. Kenny, "Ever wondered what is on the Orbcomm satellite downlink?" http://mdkenny.customer.netspace.net.au/Orbcomm.pdf, 2002.

[37] P. Misra and P. Enge, *Global Positioning System: Signals, Measurements, and Performance*, 2nd ed. Ganga-Jamuna Press, 2010.